


The ocean losing its breath under the heatwaves

Received: 6 March 2024

Accepted: 5 August 2024

Published online: 09 August 2024

 Check for updatesChangyu Li ^{1,2}, Jianping Huang ¹✉, Xiaoyue Liu ³, Lei Ding⁴, Yongli He ^{1,3} & Yongkun Xie ¹

The world's oceans are under threat from the prevalence of heatwaves caused by climate change. Despite this, there is a lack of understanding regarding their impact on seawater oxygen levels - a crucial element in sustaining biological survival. Here, we find that heatwaves can trigger low-oxygen extreme events, thereby amplifying the signal of deoxygenation. By utilizing in situ observations and state-of-the-art climate model simulations, we provide a global assessment of the relationship between the two types of extreme events in the surface ocean (0–10 m). Our results show compelling evidence of a remarkable surge in the co-occurrence of marine heatwaves and low-oxygen extreme events. Hotspots of these concurrent stressors are identified in the study, indicating that this intensification is more pronounced in high-biomass regions than in those with relatively low biomass. The rise in the compound events is primarily attributable to long-term warming primarily induced by anthropogenic forcing, in tandem with natural internal variability modulating their spatial distribution. Our findings suggest the ocean is losing its breath under the influence of heatwaves, potentially experiencing more severe damage than previously anticipated.

The global ocean has been warming and losing its oxygen primarily as a consequence of human-induced changes to the Earth's climate^{1–4}. Alongside long-term trend of increasing temperature and declining oxygen concentration, risks of extreme condition in these properties, i.e., marine heatwave and low-oxygen extreme events, has emerged in the past few decades^{5,6}. The substantial increases of these extreme signals in climate change could severely affect marine biota and ecosystems, which is recognized as a serious threat to sustainable future for the ocean and related human communities^{7–10}.

Currently, an increasing number of studies investigated the impact of global warming on declining oxygen concentrations (i.e., ocean deoxygenation) over decadal and multidecadal periods^{11,12}. The long-term warming is anticipated to reduce the solubility of oxygen and enhance biological consumption, and the warming-induced strengthening of stratification would lead to reduced ocean ventilation and a subsequent decrease in oxygen supply to the ocean

interior^{13,14}. There is also a rapidly burgeoning literature focusing on extreme warming events in the ocean, defined as marine heatwaves, which could cause widespread biological and socio-economic impacts^{15–19}. Research on low-oxygen extreme events started relatively late, but these events have received increasing attention in recent years. Characterized by the abrupt oxygen decline in the ocean, the low-oxygen extreme events could cause species to reach their critical oxygen limits decades earlier than expected from the deoxygenation²⁰, eventually resulting in the loss of biodiversity and habitats⁸. The emergence of these low-oxygen extreme events is influenced by multiple factors, including anomalous water mass distributions and ocean eddies etc.^{5,21}. Importantly, case studies have suggested that marine heatwaves may act as catalysts for extreme low-oxygen events: the abnormally low dissolved oxygen levels were found during a strong marine heatwave known as “the Blob”²². In SW Atlantic, a marine heatwave with sea surface temperatures over 30 °C coincided

¹Collaborative Innovation Center for Western Ecological Safety, Lanzhou University, Lanzhou, China. ²School of Civil Engineering and Mechanics, Lanzhou University, Lanzhou, China. ³School of Atmospheric Sciences, Lanzhou University, Lanzhou, China. ⁴Institute of Disaster Prevention, Beijing, China.

✉ e-mail: hjp@lzu.edu.cn

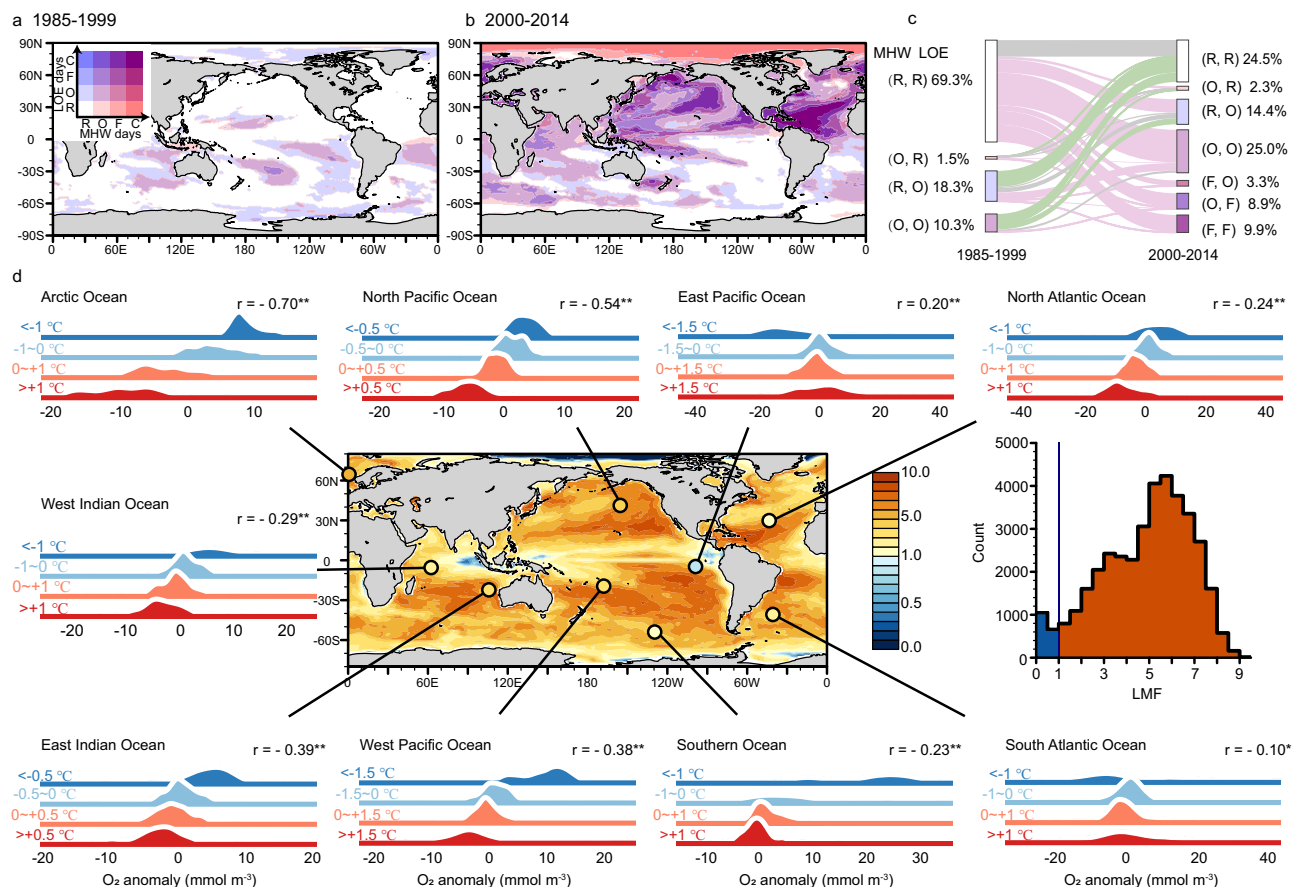


Fig. 1 | Relationship marine heatwave (MHW) and low-oxygen extreme (LOE) event. **a** Joint distribution of the annual number of event days over period 1985–1999 in ocean surface layer. **b** Same as (a) but for period 2000–2014. **c** Evolution of the two extremes from period 1985–1999 to 2000–2014. For sake of comparisons, the number of days for each extreme event type is classified into four levels, that is, Rare (R), Occasional (O), Frequent (F), Common (C), respectively, from which we could therefore obtain 16 (4*4) groups in the joint distribution. **a–c** are all derived from model simulations. **d** Maps of the likelihood multiplication

factor (LMF) based on the simulation (contour) and observation (colored dots). Warm color indicates LMF larger than 1 and the cold color opposite. Ridgeline plots depict the observed distribution of dissolved oxygen anomalies under various temperature anomaly conditions in each basin (the anomaly is calculated relative to the mean seasonal cycle). The corresponding correlation coefficients are presented in the top right corner with symbols * and ** representing the statistically significant at $P < 0.1$ and $P < 0.01$ level, respectively. The right side in (d) presents histogram counting the LMF across the ocean grids in the simulation.

with the first regional record of hypoxia²³. Observations on the Baltic Sea reveal heatwaves can contribute to seawater oxygen deficiency, especially in the shallow areas²⁴. These researches highlight the importance of exploring the coupling between heatwaves and extreme low-oxygen events. Many marine ecosystems are highly vulnerable to multiple stressors and as a consequence may suffer more severe damage if low-oxygen extreme and heatwave occur simultaneously or in close spatiotemporal proximity, as such joint occurrence has the potential to act synergistically, leading to mutually reinforcing impacts on the marine organisms^{25,26}. The combination of high water temperature and low oxygen concentration has exerted influences on marine life such as fishes and scallops^{27–29}. Nevertheless, so far we still lack a detailed knowledge about how heatwave and low-oxygen extreme coupling across the ocean. A global assessment of the modification of the compound events, as well as the drivers behind them, is urgently needed under ongoing climate change.

To fill this gap, here we conduct a comprehensive analysis of the relationship between marine heatwaves and low-oxygen extreme events in the global ocean, using in situ observations and a fully coupled Earth system model³⁰ (Data descriptions and validations of model could be found in “Methods”). The evolutions of the compound events of the two extreme events are investigated in our study and a framework is established to identify the drivers contributing to their occurrences. We focus on extreme events within the uppermost ocean

layer (0–10 m) because conditions in the surface ocean, such as temperature and oxygen levels, exert profound influences on marine ecosystems, encompassing fish populations, as well as the marine biodiversity^{23,27}. Following the approach developed in ref. 5, extreme events in temperature (oxygen concentration) are defined as a prolonged instance with anomalously warm (low-oxygen) water (See “Methods” for the detailed definitions). We expect our findings to further deepen the understanding of the synergy of extreme events in the oceans.

Results

Our results suggest that regions with relatively high frequency of heatwaves tend to suffer a highly frequent occurrence of low-oxygen extreme events (Fig. 1). The ridgeline plots present the observed temperature and oxygen concentration anomaly since the 1960s, from which we can see significantly negative correlations between the two variables in most ocean regions. The correlations between temperature and oxygen concentration anomalies become less negative yet remain evident after data detrending, as detailed in Supplementary Note 1. Outputs from a climate model provide a more detailed and clearer evidence: the joint distributions of the two type of extremes show apparent overlaps between regions with marine heatwave and with low-oxygen extreme events, which indicates the spatial patterns of annual number of event days are highly coherent across the two

types of extreme events (Fig. 1a, b). This relationship could also be found in the global patterns of individual extreme events (Supplementary Fig. 1): the pattern of low-oxygen extreme event frequency and duration broadly resembles that of marine heatwave events, with pattern correlation coefficients over 0.8 ($p < 0.01$). More importantly, both of the observations and model simulations reveal the impact of climate change on these extreme events is becoming progressively evident at the global scale, with an approximate increase in 0.07–0.09 months per year (Supplementary Fig. 2). In the late 20th century, only 10% of the world's oceans are subject to 'occasional' occurrence of both heatwave and low-oxygen extreme events, but by the early 21st century they have expanded to 24.5%; conversely, over half of the global ocean (–69.3%) is under 'rare' occurrence of the two extreme conditions during period 1985–1999, while it drops sharply to about one quarter after year 2000 (Fig. 1c). The apparent connections between the two types of extreme events can be found in both duration and frequency, visualized through purple-colored regions in Supplementary Fig. 3. Most proportion experiences an increase in both two types of the extreme hazards rather than increase in one of the single hazard type, with hotspots of largest frequency increases occurring in subtropical regions of the North Pacific Ocean and high-latitude North Atlantic Ocean (Fig. 1a, b).

All of the above results illustrate the urgency and importance of studying the synergy of the two extremes. We thereby refer to the simultaneous occurrence of extreme high temperature and low oxygen conditions in space and time as a “compound low-oxygen extreme and heatwave” event (CLH event, see “Methods”). For the daily-mean model outputs, the duration for each CLH event is calculated at in each grid cell and then used as a basis to figure out the annual statistics such as the frequency of the events, annual mean duration and total number of CLH days per year. The analysis of observation-based data is limited to basin-scale and the monthly time step due to a relatively insufficient spatial-temporal coverage. Furthermore, the likelihood multiplication factor (LMF, see “Methods”) is defined here to quantify the likelihood that a day (or month) is under CLH conditions relative to the likelihood assuming heatwaves and low-oxygen extreme events would occur independently from each other^{31–33}.

The features of the LMF reveal statistical dependencies between marine heatwaves and low-oxygen extremes. The observational data indicates a globally averaged LMF of approximately 4.0. This implies a strong positive correlation between the two type of extreme events and, likewise, that the co-occurrence of the two extremes (i.e., CLH event) would be four times more frequent than the situation expected if heatwave and low-oxygen extreme were statistically independent. For the basin scale, the observed LMFs are larger than 1 in almost all of the ocean regions except the Eastern Pacific (colored dots in Fig. 1d). Model simulations are in good agreement with the observations, showing that over 90% of the ocean experience more CLH events (i.e., $\text{LMF} > 1$, contour lines in Fig. 1d), with a global average LMF value of approximately 5.1. Furthermore, the simulations reveal distinct LMFs among the global ocean due to differences in their intrinsic driving mechanisms. The largest LMF (> 5) occurs in the subtropical regions such as mid-latitude Pacific and Atlantic Ocean, indicating strong correlations between the two extremes in these regions, while the $\text{LMF} < 1$ in the equatorial East Pacific and Indian ocean in which relatively less probability of CLH events occurrences exist. We further perform the LMF analysis after detrending the data, serving as a sensitivity analysis within our study. The details can be found in Supplementary Note 1, illustrating the impact of temperature and oxygen concentration trends on the LMF of CLH events and demonstrating the robustness of our results.

The evolutions of CLH event reveal substantial modifications as a consequence of climate change (Fig. 2b). The annually observed number of months with CLH events has significantly risen in the majority of the oceans (Supplementary Fig. 4). Comparisons between

two 15-year periods (1985–1999 and 2000–2014) in the climate model also show a considerable rise in annual CLH days, with increases in more than 70% of the world's ocean and a global average increase exceeding 20 days, despite large spatial variations exist (Fig. 2c). The largest enhancement occurs in the mid-latitude ocean basins, with an increase of up to 100 days. Decreases in annual CLH days are found in parts of the eastern tropical Pacific and high-latitude Southern Ocean. As a global average, the annual CLH days have increased significantly in the past few decades, with a linear trend of +0.96 days per year ($p < 0.01$; Fig. 2b, purple line). By the 2010s, the global ocean increases by approximately 25 additional CLH days per year compared with a baseline level of 14 days in the 1980s. This increase in annual CLH days indicates either an increase in the frequency of CLH, a prolongation of event duration, or an increase in frequency in conjunction with a prolongation of duration. Supplementary Fig. 5 shows the characteristics of CLH frequency and annual mean duration, from which we can see the distinct contributions of the two variables to the increases of annual CLH days in different regions. The detailed discussions about the contribution of frequency and duration changes to the increase of annual CLH days can be found in Supplementary Note 2.

It should be specifically noted that, alongside the increasing number of event days, the low-oxygen extreme events are becoming increasingly associated with heatwaves over the past few decades: during the period 1970–1984, about 41.0% of the low-oxygen extreme days are accompanied with heatwave globally, while it increases to 45.5% in 1985–1999 and eventually exceeds over 50% in 2000–2014 (Venn diagram in Fig. 2b). In other words, there is one out of every two low-oxygen extreme days that simultaneously suffers extremely high temperatures in the early 21st century. At the regional scale, the strengthening of coupling can also be found in most oceanic basins except for the East Pacific Ocean, although slight difference exists in the magnitude (percentages in Fig. 2c). The joint occurrences (i.e., CLH events) have become the dominant concern in the evolution of low-oxygen extreme events, reflecting a substantial increase in its synchronization with heatwaves.

The increasing co-occurrence of heatwave and low-oxygen extreme could have far-reaching implications for human society. Here we present the characteristics of CLH events in four representative fishing waters (i.e., The North Sea, Hokkaido fishing zone, East China Sea and Newfoundland fishing zone, Fig. 3a–i). Comparisons between two periods (1970–1984 and 2000–2014) reveal that these regions suffer a significantly longer persistence of both extreme high-temperature and low-oxygen conditions under climate change (Fig. 3a, c, f, h). There has also been an apparent enhancement of extreme event intensity in these fishing zones over the last few decades. The associated temperature and oxygen concentration anomalies show that CLH events after 2000 bring extreme conditions of much higher temperatures (+13%) and lower oxygen concentrations (–11%) than those before 2000 (Fig. 3b, d, g, i). It is also noteworthy that the response of CLH events to climate change is more sensitive in regions with abundant fish biomass than in other marine areas. In combination with global ocean biomass map^{34,35}, we found that the most substantial average increase in annual CLH days occurs in ocean regions with high fish biomass (Fig. 3j). In regions where fish biomass exceeds 50 gm^{-2} , there is an upward trend of CLH days about 1.47 days per year. The rise is approximately 50% greater than the global average increase. Specifically, the increase in annual CLH days in the North Sea, Hokkaido, East China Sea, and Newfoundland fishing zones is +3.64, +2.95, +2.66, and +3.34 days per year, respectively, all of which are more than 2.5 times the global average (approximately +0.96 days per year). Only 8% of the ocean where fish biomass below 5 gm^{-2} suffers an increase of CLH days larger than the global average level. In contrast, this percentage rises to 66% in the ocean regions where fish biomass exceeds 200 gm^{-2} . Fish biomass declines more rapidly with increasing trends of CLH days under climate change (Supplementary Fig. 6). This greater increase of

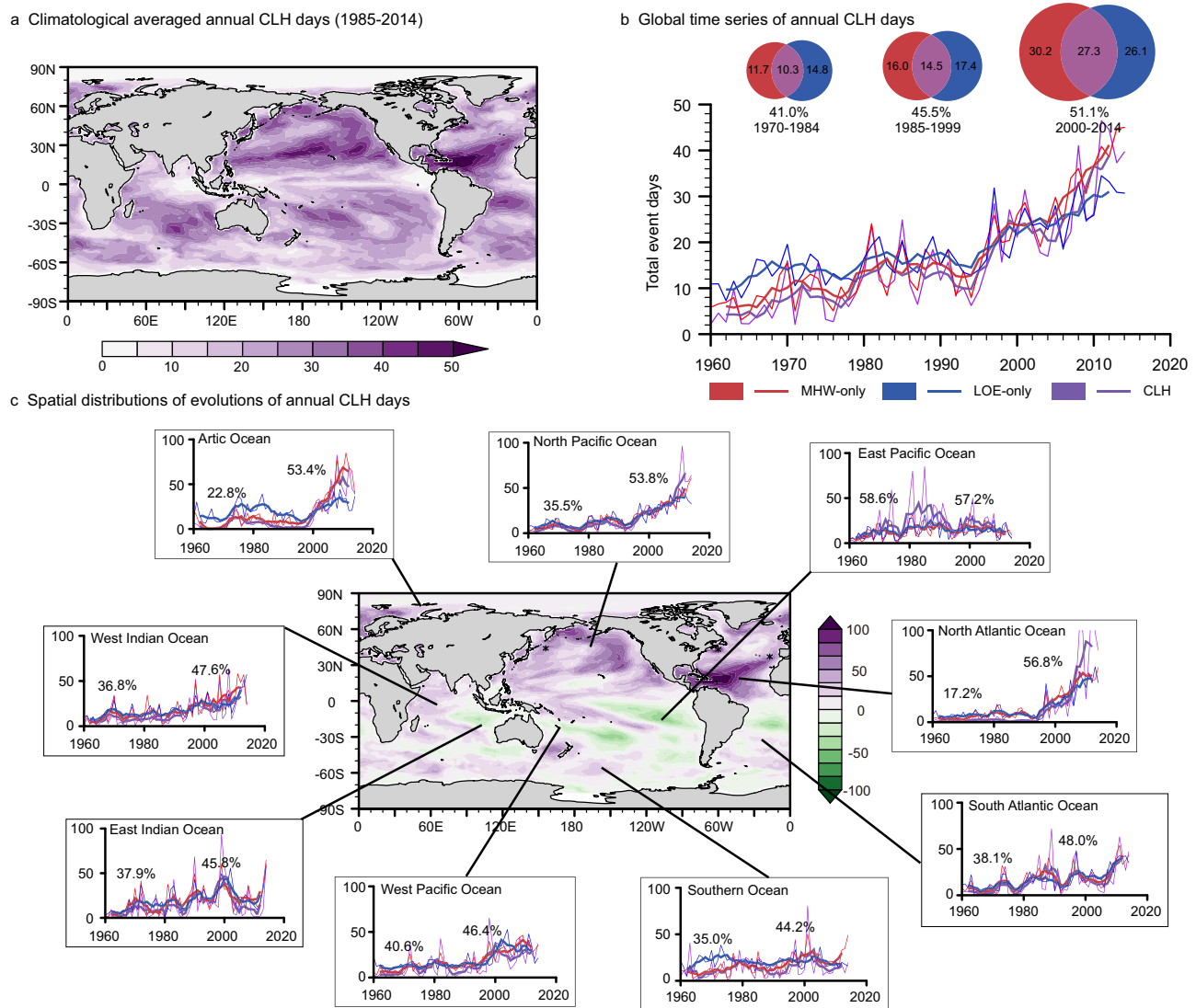


Fig. 2 | Annual event days for compound low-oxygen extreme and heatwave (CLH), marine heatwave only (MHW-only) and low-oxygen extreme only (LOE-only) in ocean surface layer based on the model simulations. a Climate average spatial distribution of annual CLH days over the 1985–2014 period. **b** Global time series of annual total days for CLH, MHW-only and LOE-only. Note that the thick solid lines are 5-year running averaged time series. The percentages present the ratio of CLH and LOE days (note that LOE days are the sum of CLH and LOE-only days) over the given time period. Days that only marine heatwave occurs are

colored in red; similarly, that only low-oxygen extreme occurs are colored in blue. The CLH days that low-oxygen and marine heatwave occur simultaneously are colored in purple. **c** Spatial distributions of annual CLH day changes. The curve plots are same as **(b)** but for nine ocean basins. Specifically, the two percentages represent the ratio over 1960–1984 and 1990–2014, respectively. Contour plot represents difference of the annual CLH days between the 1985–1999 and 2000–2014.

CLH events in high-biomass regions implies more severe damage to marine life and ecosystem, which may eventually influence human communities that rely heavily on fisheries, especially for those coastal regions in developing countries. It should be noted that low-resolution climate models such as CESM are recognized for exhibiting biases in coastal regions due to their limited ability to capture small-scale processes such as boundary currents, coastal dynamics, and ocean eddy fluxes³⁶. Previous study has revealed an underestimation of marine heatwaves in CESM within coastal regions throughout the historical period³⁷. In other words, the actual conditions in coastal regions might be more severe than anticipated in our manuscript. This underscores the pressing need for high-resolution models operating at daily time-scales to explore extreme events in biomass-rich coastal oceans.

A systematic assessment of the drivers behind these changes is necessary and urgently needed. For this purpose, here we employ the ensemble empirical mode decomposition (EEMD), an adaptive one-

dimensional time series analysis method that separates scales naturally without any prior subjective criterion³⁸ (see “Methods” for detailed descriptions). As demonstrated in previous studies^{39–41}, the EEMD method can effectively separate anthropogenic forcing signal from natural internal variability in the time series. For example, based on this method, we can split the time series of global averaged seawater temperature as well as oxygen concentration into relatively short-lived and transient oscillation component associated with natural internal variability and long-term warming signal primarily related to anthropogenic forcing, as depicted in Supplementary Fig. 7. For multi-dimensional spatial–temporal temperature and oxygen concentration data, the EEMD method is applied into each grid cell to obtain the long-term signal as well as the oscillation component for these variables. Following ref. 39, We then piece together the oscillation components from all grid cells to create a gridded dataset which constructs a temporal evolution of the spatially coherent structure of this

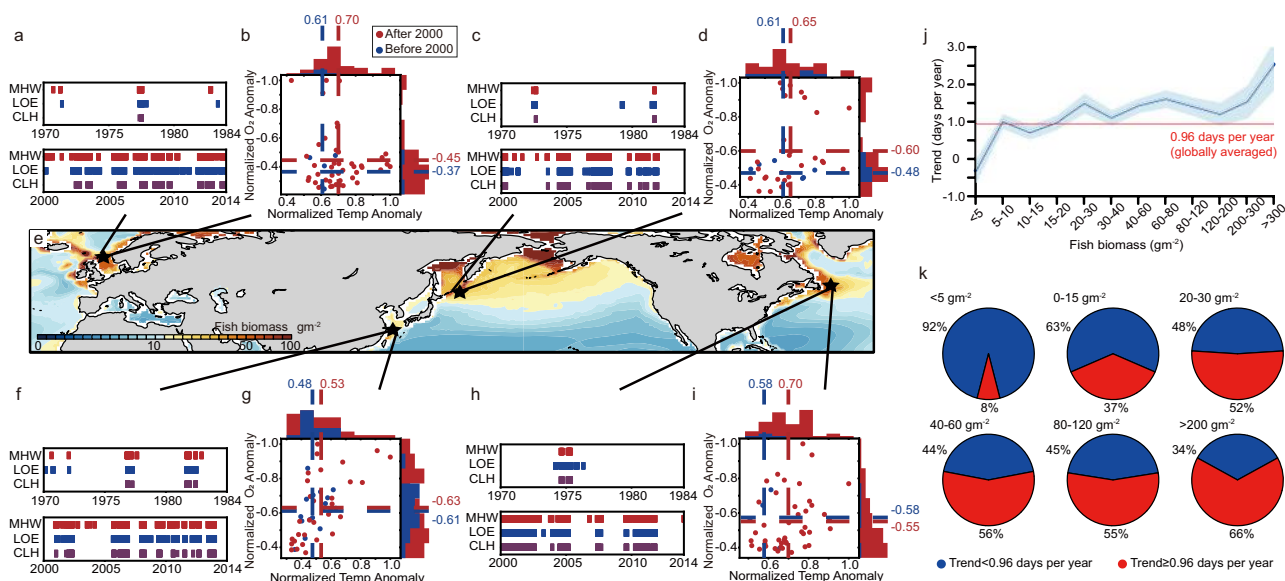


Fig. 3 | Compound low-oxygen extreme and heatwave (CLH) events in relationship with marine fish biomass. Features of extreme event in four representative fishing waters (**a, b**, The North Sea; **c, d**, Hokkaido fishing zone; **f, g**, East China Sea; **h, i**, Newfoundland fishing zone). **a, c, f, h** The persistence of extreme events in 1970–1984 and 2000–2014 (marine heatwave (MHW) colored in red, low-oxygen extreme (LOE) colored in blue and CLH colored in purple). **b, d, g, i** Intensity of CLH event before (blue) and after (red) year 2000. **e** Spatial pattern of marine

fish biomass (g m^{-2}). **j** The linear trend of annual CLH days during period 1985–2014 as a function of the fish biomass. **k** the percentages of regions exhibiting an annual trend of CLH days exceeding (red pie charts) or falling (blue pie charts) below global average (0.96 days per year) within six biomass groups. In (**b, d, g, i**) each dot represents a CLH event, and the blue (red) dashed line is the averaged intensity of these events before 2000 (after 2000). The CLH events are identified based on the condition of the ocean surface layer, which are derived from model simulations.

component. Eventually, we can obtain the spatiotemporal evolution of extreme events related to natural internal variability by conducting extreme event detection on this dataset. Similar methodologies are employed on the long-term signal to investigate the impacts of anthropogenic forcing. By using this EEMD-based method, we can thereby obtain the characteristics of extreme events under influence of natural internal variability and long-term signals.

Figure 4a illustrates the annual changes in CLH days associated with the long-term warming and oxygen decline caused by anthropogenic forcing. It can be seen that the vast majority of the world's oceans are facing an increase in the number of CLH days since the 1980s, with some regions experiencing an increase of more than 50 days (Fig. 4a). This spatial pattern is directly shaped by the concurrent trends of warming and decrease of oxygen concentration. For example, certain regions in the North Pacific exhibits the highest values, indicating that these oceans experience the most pronounced concurrence of temperature increase and oxygen concentration decline.

The CLH events related to relatively short-lived and transient oscillation component can be caused by the interaction of many local and remote processes and phenomena acting across a large range of temporal and spatial scales. The underlying mechanisms are highly intricate. The strength of many of local processes (e.g., heat fluxes and vertical mixing) are a function of the overlying atmospheric synoptic conditions. These conditions fluctuate in response to shifts in the general circulation and internal climate variability, such as El Niño–Southern Oscillation (ENSO) and Indian Ocean Dipole (IOD), across the globe. Therefore, the contribution of natural internal variability significantly varies by location. It has a positive impact on annual CLH days in widespread North Pacific and North Atlantic oceans during period 2000–2014, while negative impact is found in regions such as Equatorial Pacific and Southern Ocean (Fig. 4b). Based on method developed by ref. 42, we further explored the occurrence of extreme events in relationship with various modes of internal climate variability which have characteristic time scales ranging from sub-seasonal (e.g., the Southern Annular Mode, SAM) to multidecadal (e.g.,

the PDO), as these climate modes act to modulate the local conditions—either from local sources or remote sources via teleconnection mechanisms. Their relationships are quite complex, but we can still find clear patterns consistent with the known temperature or pressure patterns (Fig. 4c; Supplementary Figs. 8, 9). For example, ENSO seems to be the main modulator of CLH in the East Equatorial Pacific as well as Northwest Indian Ocean; the SAM dominates the occurrence of CLH event in vast ocean south of 40°S; the IOD, represented by Dipole Mode Index (DMI), strongly relate to CLH events around Indonesia. The region of North Atlantic in 30–50°N is very interesting that this region is influenced by various climate modes, including NAO (Supplementary Fig. 10). However, the influence of NAO is relatively minor compared to other modes; hence it is not drawn in the figures.

Our results reveal that both anthropogenic forcing and natural internal variability are responsible for the modifications of CLH events: the former is the main contributor to the lengthening of annual CLH days at the global scale, while the latter plays an important role in spatial distributions of this change. For instance, mid-latitude oceans, including the North Pacific and North Atlantic, experience substantial influence from the long-term warming signals driven by anthropogenic forcing, as well as variability modulated by climate modes such as PDO (Fig. 4). The collective impact of these factors has contributed significantly to a noteworthy increase in CLH days within mid-latitude oceans. It's worth noting that the signals separated by the EEMD method are generally considered to be caused by anthropogenic forcing and internal climate variability. We acknowledge that our method does not identify specific signals such as aerosols and volcanic activities. Further attribution analysis is needed to disentangle the contributions of various factors in the future.

A range of mechanisms can lead to coherent synergy of anomalously warm and low-oxygen waters. Temperature variations may result from a confluence of processes, including air-sea heat exchanges, current and eddy-driven advection, horizontal and vertical mixing, as well as the entrainment of water into the surface layer¹⁹. For the oxygen concentration, changes in oxygen solubility due to sea surface temperature variations plays a crucial role in modifying the seawater's

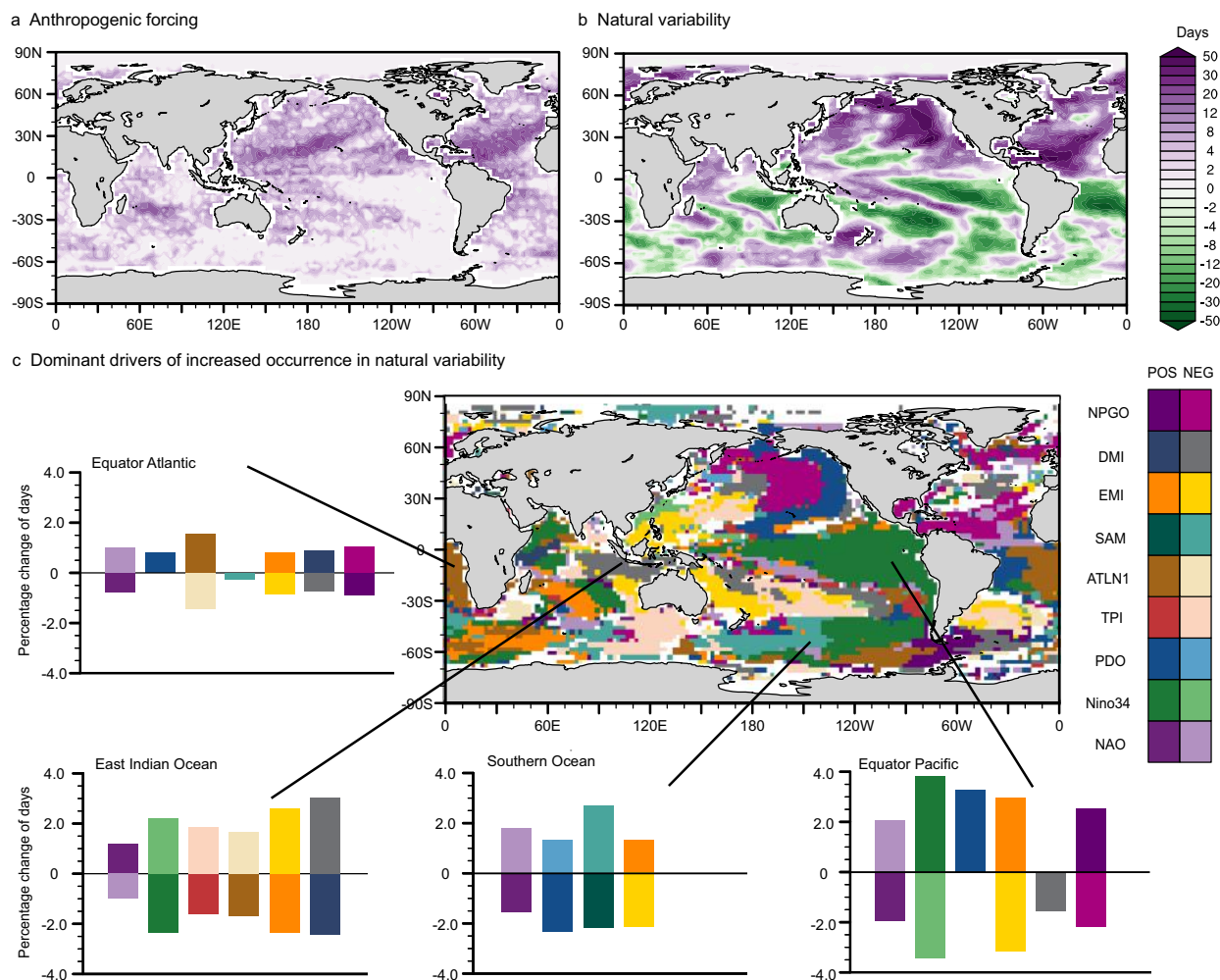


Fig. 4 | Drivers of compound low-oxygen extreme and heatwave (CLH) event evolution. a, b The contribution of anthropogenic forcing and natural variability to the changes of annual CLH days (calculated as the difference between period 2000–2014 and 1985–1999) in the ocean surface layer. **c** The dominant climate patterns that modifies CLH event in natural variability. The map provides

information about which climate modes and phases (positive or negative) have greatest impacts on increase of CLH event over the period from 1985 to 2014. The bar charts show percentage change of CLH event days linked to phase of climate patterns in a certain ocean region. The results in this figure are derived from model simulations.

capacity to store oxygen. Concurrently, the air-sea oxygen flux, along with the horizontal and vertical transport of dissolved oxygen as well as local processes of oxygen production and consumption, collectively shape surface dissolved oxygen concentrations. These processes mentioned above are subject to modulation by local and remote factors operating over a broad spectrum of spatial and temporal scales. The strength of many of these processes are a function of the overlying atmospheric synoptic conditions. These conditions fluctuate in response to shifts in the general circulation and climate variability, such as ENSO, PDO, and IOD, as well as the human-induced long-term changes across the globe⁴². Under the combined dominations of natural internal variability and anthropogenic climate change, These modifications lead to the accumulation of heat and eventually outbreak of heatwave^{19,43}. This extreme high temperature simultaneously reduces the solubility of dissolved oxygen, which directly cause oxygen escape from ocean^{10,44}. For further validation, we investigated the changes in oxygen solubility during extreme events (Supplementary Fig. 11a). The oxygen solubility in seawater during CLH events exhibits an apparent decrease compared with the average state, indicating a reduced capacity of seawater to store oxygen. Interestingly, enhanced stratifications, indicated by mixed layer shallowing, occurs in the ocean during the events (Supplementary Fig. 11b). This intensified ocean stratification can hinder the ventilation of oxygen¹³, suppress

the ocean's oxygen supply, which might eventually affect oxygen in the ocean interior.

Discussion

A shift characterized by warming and deoxygenation has been occurring in widespread ocean under climate change^{45,46}. Recorded as “peak signal” in this process, the associated extreme events can deteriorate the living environment within a relatively short timeframe, resulting in devastating impacts on marine ecosystems and biota. Here we find the low-oxygen extreme events are becoming increasingly associated with heatwaves. Occurrence of heatwave becomes more frequent in the warming world, which meanwhile boosts low-oxygen extreme events. Importantly, our results of a marked increase in CLH frequency, intensity as well as annual days implies that marine ecosystems are increasingly subject to suffer multiple physical and biochemical stressors simultaneously rather than single hazards²⁸. We further clarify the contributions of anthropogenic forcing and natural variability to the lengthening of annual CLH days, with the former being the primary contributor at global scale and the latter significantly influencing the spatial distribution of these changes. Our findings underscore the potential for heightened compound extreme risks to marine ecosystems, necessitating proactive planning in adaptation strategies for future climate-linked hazards.

Methods

Dissolved oxygen and temperature observations in the ocean

We use in situ observations from World Ocean Database (WOD) 2018, the world's largest collections of the uniformly-formatted and quality-controlled ocean profile data⁴⁷. Approximate 1.3 million profiles flagged good are selected from the database, which contain both temperature and dissolved oxygen data since 1960 (Supplementary Fig. 12). Given our primary emphasis on extreme events in the uppermost ocean layer, only profile data near the ocean surface (0–10 m) is utilized in this study. We referred to Schmidt's paper⁴ to complete a series of technical steps such as data filtering and preprocessing (quality control, duplicate removal, etc.), except that the ocean is divided into nine basins for sake of comparisons and analysis (the definition of ocean basins can be found in Supplementary Fig. 13). We first divided the ocean into grids of 2.5 degrees by 2.5° and mapped each profile data to the grid point closest to the recorded latitude and longitude at the time of observation. Then, we followed the defined basin boundaries, performed a weighted average of all eligible data based on their grid coordinates, and eventually obtained the time series for each basin. Note that this observational data is limited to monthly-mean resolution due to insufficient temporal coverage. We acknowledge that the averaging in the mapping is inevitably affected by missing values. However, limited by the spatiotemporal coverage of WOD data, this is the compromise approach we adopted after comprehensive consideration. The World Ocean Atlas (WOA) 2018, which is based on WOD18 and provides climate mean map of the temperature and dissolved oxygen, is used in this study as the reference to evaluate the model simulations.

Two additional observation-based datasets, namely the Optimum Interpolation Sea Surface Temperature (OISST)⁴⁸ dataset and the Gridded Ocean Biogeochemistry from Artificial Intelligence-Oxygen (GOBAI-O2)⁴⁹ dataset, are also employed in this study. The OISST dataset is derived from remotely sensed sea surface temperature by the advanced very high-resolution radiometer infrared satellite data and in situ measurements. It maintains a global spatial resolution of 0.25° on a daily scale since 1981. The recently published GOBAI-O2 dataset provides ocean dissolved oxygen concentrations derived through machine learning algorithms trained on oxygen concentration observations from Argo-float-mounted sensors and discrete measurements from ship-based surveys. It covers the period from 2004 to 2022 with a monthly 1° × 1° resolution. For our study, both the OISST and GOBAI-O2 datasets are processed to a consistent spatial and temporal resolution and specific overlapping time periods when both datasets are available.

Descriptions of the climate model

The global analysis of extreme events was mainly conducted with outputs derived from the fully-coupled Community Earth System Model (CESM, version 2.1.3) developed at National Center for Atmospheric Research (NCAR)³⁰. The CESM consists of ocean, atmosphere, land, sea-ice, land-ice, river, and wave models, which could provide state-of-the-art computer simulations of the Earth's climate states. For the ocean component, the description of physical process is based on the Parallel Ocean Program version 2 (POP2) and the ocean biogeochemistry is simulated by Marine Biogeochemistry Library (MARBL). The ocean has a normal 1° × 1° horizontal resolution (gradually increasing toward the Equator), and 60 vertical levels. In this study, Our CESM experiment is the same as the CMIP6 historical experiment⁵⁰. As a result, the forcings are based on observations from 1850 to 2014 and include greenhouse gas emissions, land-use conditions, solar forcing, and so on. The forcing data, in particular, were officially provided by the CESM group, as introduced by Danabasoglu et al.³⁰ in Section 5. Only the last 55 years of the historical experiment (i.e., 1960–2014, period when the intensity of human activity increases dramatically) is used for validations and analysis.

Definition of extreme and compound extreme events

A seasonally varying climatological threshold is used to define the extreme event, that is, the temperature above 90th-percentile threshold for marine heatwave (extremely high-temperature event)^{15,51} and the oxygen concentration below 10th-percentile threshold for low-oxygen extreme^{5,21}. In this study, the percentile threshold is calculated over the full range of the time series studied in our manuscript, that is, from year 1960 to 2014, and determined from the shortest available time-step, i.e., monthly for observations and daily for the model simulations. For each grid cell or ocean basin, we separately calculate the threshold for each calendar day (model outputs) or month (observation data) of a year. To ensure the continuity of extreme events, for the daily time series, a duration of at least 5 days with temperature above the threshold (oxygen concentration below the threshold) is imposed in the identification of an extreme event, and two events separated by an interval of two or fewer days are considered as one event.

The compound low-oxygen extreme and heatwave (CLH) events are defined as the days or months when extremely high-temperature and low-oxygen conditions occur simultaneously (that is, both temperatures above 90th-percentile and oxygen concentration below 10th-percentile at the same time and location). Similar to marine heatwave and low-oxygen extreme events, we also impose a criterion on the minimum duration of this compound event, with the caveat that it is slightly shorter compared with the individual extreme event, specifically 2 days. The annual statistics for CLH events, such as event frequency, annual mean duration, and the total number of extreme days per year, are calculated in the same manner as marine heatwaves.

Evaluation of model simulations against in situ observation

Comparisons with WOD18 and WOA18. We firstly evaluate the simulated oceanic dissolved oxygen and temperature in comparison with the observational data from WOD18. As shown in Supplementary Figs. 14, 15, the model is able to capture the observed temperature and dissolved oxygen patterns. For the climate mean state, the model simulates well the distribution of temperature and dissolved oxygen concentration among the ocean basins. It should be noted that, similar with results from other CMIP-type models³⁶, bias exists in the our CESM outputs. A Lower temperature, about −0.42 °C on average, is simulated in some high-latitude regions compared with observations, while the opposite is found in part of central-eastern Pacific and Atlantic, approximate +0.39 °C on average. The simulated dissolved oxygen exists bias mainly in Extra-equatorial ocean, where the model overestimates oxygen concentration with an average of approximate +4.69 mmol m^{−3}. Nevertheless, the simulated distribution is in good agreement with it in observations from WOA 2018, with pattern correlation coefficient over 0.90, significant at 0.01 level. More importantly, the model captures very well the temporal evolution of the extreme and compound extreme events under climate change (Supplementary Fig. 2). The marine heatwave is simulated to increase by 0.09 ± 0.01 month per year since the 1960s, which corresponds well with the observed trend of 0.07 ± 0.01 month per year. Besides, both the model and observation reveal an increase in low-oxygen extreme events, approximate 0.09 ± 0.01 month per year over 1960–2014. Accurate simulations of the heatwave and low-oxygen extreme events eventually lead to a very good agreement between simulated CLH event and the observation-based characteristics.

Comparisons with OISST and GOBAI-O2. We also assess the model simulations against the results from OISST and GOBAI-O2 datasets. Supplementary Figs. 16, 17 include climatology comparisons between the simulation and observation. This analysis spans the timeframe when data are concurrently available in both observation datasets and model simulations. The bias and root mean square error (RMSE) metrics for sea temperature reveals that, overall, the simulation

performs well, with biases typically less than 1 °C. Noteworthy exceptions, such as Kuroshio, North Atlantic coast, equatorial South Africa, Peru coast, California coast, have been identified and discussed in earlier studies. The distribution of RMSE is consistent with that of bias. The larger bias corresponds the large value of RMSE. Therefore, the simulation has a good performance to capture the variation of sea surface temperature. Supplementary Fig. 17c illustrates that the bias for oxygen concentration is generally less than 15 mmol m⁻³, representing approximately 10% relative to the climatology. Despite larger biases observed in specific regions, such as the Indian Ocean and high latitudes of the Atlantic and Pacific Oceans, we think that these discrepancies fall within an acceptable range for investigating oxygen variation. The distribution of RMSE between simulation and observation aligns with that of bias, with the majority of values being less than 20 mmol m⁻³. We consider such bias acceptable for investigating the variation in oxygen levels.

The trend distribution of Seawater temperature and oxygen concentration is illustrated in Supplementary Figs. 18, 19. In general, the simulated temperature trend aligns well with the observations, although the trend of seawater temperature in the North Pacific is overestimated, and in the South Pacific, it is underestimated. The bias of trend in the Atlantic is much less than that in Pacific. Regarding oxygen concentration, the simulations indicate an overall decline in most ocean regions, which is consistent with the observations, despite that the simulation overestimated the decreasing trend in the Pacific and underestimated the increasing trend in the Atlantic, and in the southern hemisphere, the increasing trend in dissolved oxygen concentration contrasts with the observed decreasing trend. The temporal correlation coefficients between the observed and simulated seawater temperature, as well as dissolved oxygen concentration, were investigated in Supplementary Fig. 20. The results suggest that the correlation coefficient exceeds 0.9 in most regions, except for certain oceanic areas near the equator. This finding highlights a noteworthy coherence between the observed time series of seawater temperature and oxygen concentration and those derived from simulations.

We explore the spatial distribution characteristics of CLH events using observation-based data and compare them with model-derived simulations, as depicted in Supplementary Fig. 4. Notably, the time resolution of GOBAI-O2 is monthly, thus the unit for observation-based annual CLH days is denoted as “months per year”. For the purpose of comparison in Supplementary Fig. 4, we convert this unit to “days per year” by assuming a factor of 30 days per month. Due to limitation of temporal coverage of GOBAI-O2 dataset, the trend of annual CLH days for observation is calculated for period 2004–2022. The simulated climatology of annual CLH days exhibits remarkable similarity to that derived from observations, with a pattern correlation of 0.84. Regions with the most pronounced annual CLH days are situated in the North Pacific, mid-latitude North Atlantic, and certain areas in the South Indian Ocean. Despite existing differences, both simulations and observations indicate a global increase in annual CLH days. A significant upward trend is found in the North Pacific and the vast Atlantic Ocean in both simulations and observations. Increases in annual CLH days are also evident in regions of the Indian Ocean and Southern Ocean, although the rise in simulations is generally less pronounced than in observations.

The comparisons between the high temporal resolution model simulations and observational data also suggests that the feature of extreme events is relatively insensitive to the temporal resolution. The great consistence between model and observation gives us confidence in using the climate model (CESM) to analyze the spatial and temporal evolution of ocean biogeochemical extremes and heatwaves at the global scale.

Classification of the extreme events

To present a clear description of extreme events and their joint distribution, for each type of extreme event, we firstly classified the

number of event days into four levels, that is, so-called Rare (R), Occasional (O), Frequent (F), Common (C) in our study. The thresholds dividing these four levels are the 40th, 70th, and 90th percentiles of annual event days across the oceans (Supplementary Fig. 21). After classification, the evolution of extreme events and their joint distribution are straightforward in Fig. 1a–c.

Likelihood multiplication factor

The LMF is used to illustrate the impact of the possible correlation between hazard pair (that is, marine heatwave and low-oxygen extreme) on their joint occurrence probability³², and likewise, estimate in which regions the compound events are more likely to occur³³. The LMF in this study is given by:

$$LMF = \frac{P(\text{cooccurrence of heatwave and low oxygen extreme})}{P(\text{heatwave}) \times P(\text{low oxygen extreme})} \quad (1)$$

the ratio of actually observed probability of joint occurrence (i.e., CLH event) and probability assuming the two types of extreme events complete independence.

Depending on the relationship between the hazards pairs, the LMF can range from 0 to an upper limit defined by percentile thresholds (it is 10 in our manuscript). An IMF higher than 1 indicates compound event occurs more often than by chance, and likewise, that there is a positive dependence between heatwave and low-oxygen extremes, with the value increasing with the strength of correlation. In contrast, LMF less than 1 suggests that the two types of extreme are negatively correlated, that is, a reduced likelihood of compound event. The LMF is calculated for each grid cell (model outputs) and each ocean basin (model outputs & observations) in this study.

Ensemble empirical mode decomposition method

The EEMD is an adaptive one-dimensional time series analysis method that separates scales naturally without any prior subjective criterion⁵². This noise-assisted technique could perform operations that partition a series into different ‘modes’:

$$X(t) = \sum_{i=1}^n IMF_i(t) + r(t) \quad (2)$$

where IMF_{*i*} is the *i*th Intrinsic Mode Function (IMF) which are oscillatory components with distinct frequencies and amplitudes and *r*(*t*) is the residual part of the data after all the IMFs have been extracted.

In this study, the EEMD is used to separate signals of anthropogenic forcing and natural internal variability in the evolution of extreme events. Time series of sea temperature and oxygen concentration are decomposed via the EEMD method for each grid cell. We set the amplitude of added noise to 0.2 times the standard deviation of the original data. The ensemble number is 400 and the total number of IMFs is 6. Following ref. 40, the sum of IMF 1–5 is treated as the relatively short-lived and transient oscillation components related with natural internal variability and IMF 6 is the long-term signal for anthropogenic forcing.

Using the EEMD method, the original time series is decomposed into two components: the anthropogenic forcing signal and the internal natural variability signal. By performing extreme event detection on the anthropogenic forcing signal, we can identify extreme events related to anthropogenic factors. Similarly, extreme events related to natural internal variability are identified by conducting extreme event detection on the latter.

An important clarification can be found in Supplementary Note 3 to perceive the underlying consistency between the results from EEMD-based method in our study and the shifting baseline approach suggested by Amaya et al.⁵³. The principles underlying the EEMD-based method resonate with the fundamental concept articulated by Amaya et al. (2023), which highlights the need for separation of influence of

long-term signal and relatively short-lived and transient changes on extreme events.

Attributions to large-scale modes of climate variability

An analytical framework established by Holbrook et al.⁴² is used in this study to identify regions where there is a statistically significant relationship between the occurrence of CLH events and the internal natural variability represented by large-scale climate modes. This framework provides a systematic approach for evaluating the impact of climate variability on extreme events, and can be applied to a wide range of data and models.

Nine commonly used climate indices are considered in this study, including Niño-3.4 index, EMI (ENSO Modoki Index), DMI, NAO (North Atlantic Oscillation) index, PDO (Pacific Decadal Oscillation) index, TPI (Tripole index), Atlantic Niño index, SAM (Southern Annular Mode) index, NPGO (North Pacific Gyre Oscillation) index (see Supplementary Note 4 for detailed descriptions). For each grid, we calculate the frequency of compound events during positive and negative phases of these key climate modes and identify which climate modes are significantly related to occurrence of CLH event following the method by Holbrook et al.⁴². In our manuscript, this framework is done by summing the number of CLH days at each location and determining whether the climate index is in a positive or negative phase. Monte Carlo simulations are conducted to determine whether the number of days counted were greater or less than what might be expected by chance. For a specific climate index, we generate a synthetic time series with autocorrelation characteristics akin to the index, utilizing a fourth-order autoregressive model. Subsequently, we recalculate the number of CLH days during positive and negative phases of the synthetic index. This process is repeated 10,000 times to produce a frequency distribution of the expected number of days. The 5th and 95th percentiles are used to form confidence intervals for the given mode and region. The climate modes (and phases) which have the greatest significant impact on occurrence of CLH event are eventually shown in Fig. 4c. By using this framework, we aim to gain a better understanding of the underlying causes of CLH events linked to internal climate variability.

Data availability

The observed oxygen concentration and temperature from World Ocean Database 2018 (WOD18) and World Ocean Atlas 2018 (WOA18) is collected and maintained by NOAA National Centers for Environmental Information (NCEI), which is available at <https://www.ncei.noaa.gov/products/world-ocean-database>. Two additional observation-based datasets, namely the Optimum Interpolation Sea Surface Temperature (OISST) and the Gridded Ocean Biogeochemistry from Artificial Intelligence-Oxygen (GOBAI-O2), are used in this study, which can be accessed at <https://www.ncei.noaa.gov/products/optimum-interpolation-sst> and <https://doi.org/10.25921/z72m-yz67>, respectively. The ocean biomass data used in this study can be accessed at <https://doi.org/10.5281/zenodo.5520055> and <https://doi.org/10.5281/zenodo.8345264>, respectively. The data underlying the analyses in this study are deposited in the Zenodo repository under <https://doi.org/10.5281/zenodo.12819499>.

Code availability

The CESM (version 2.1.3) code used for the simulations is available at <https://www.cesm.ucar.edu/>. The code used in this study to detect extreme events (e.g., marine heatwaves) is available at <https://doi.org/10.5281/zenodo.7029736>. A python module for EEMD (PyEMD) is available at <https://doi.org/10.5281/zenodo.5760057>. The code that examines relationship between extreme events and key climate modes can be accessed from https://github.com/ecjoliver/MHW_Drivers. The NCAR Command Language (NCL) is used for visualizations, which is available at <https://www.ncl.ucar.edu/>. The code to generate the

results presented in the study can be obtained from <https://doi.org/10.5281/zenodo.12819499>.

References

- Cheng, L. et al. Another record: ocean warming continues through 2021 despite La Niña Conditions. *Adv. Atmos. Sci.* **39**, 373–385 (2022).
- Oschlies, A. A committed fourfold increase in ocean oxygen loss. *Nat. Commun.* **12**, 2307 (2021).
- Li, C., Huang, J., He, Y., Li, D. & Ding, L. Atmospheric warming slowdown during 1998–2013 associated with increasing ocean heat content. *Adv. Atmos. Sci.* **36**, 1188–1202 (2019).
- Schmidtko, S., Stramma, L. & Visbeck, M. Decline in global oceanic oxygen content during the past five decades. *Nature* **542**, 335–339 (2017).
- Gruber, N., Boyd, P. W., Frölicher, T. L. & Vogt, M. Biogeochemical extremes and compound events in the ocean. *Nature* **600**, 395–407 (2021).
- Hauri, C. et al. More than marine heatwaves: a new regime of heat, acidity, and low oxygen compound extreme events in the Gulf of Alaska. *AGU Adv.* **5**, e2023AV001039 (2024).
- Cheung, W. W. L. et al. Marine high temperature extremes amplify the impacts of climate change on fish and fisheries. *Sci. Adv.* **7**, eabh0895 (2021).
- Köhn, E. E., Münnich, M., Vogt, M., Desmet, F. & Gruber, N. Strong habitat compression by extreme shoaling events of hypoxic waters in the Eastern Pacific. *J. Geophys. Res. Oceans* <https://doi.org/10.1029/2022jc018429> (2022).
- Wishner, K. F. et al. Ocean deoxygenation and zooplankton: very small oxygen differences matter. *Sci. Adv.* **4**, 1–9 (2018).
- Li, C. et al. Increasing escape of oxygen from oceans under climate change. *Geophys. Res. Lett.* **47**, e2019GL086345 (2020).
- Bopp, L. et al. Multiple stressors of ocean ecosystems in the 21st century: projections with CMIP5 models. *Biogeosciences* <https://doi.org/10.5194/bg-10-6225-2013> (2013).
- Gong, H., Li, C. & Zhou, Y. Emerging Global ocean deoxygenation across the 21st Century. *Geophys. Res. Lett.* **48**, e2021GL095370 (2021).
- Oschlies, A., Brandt, P., Stramma, L. & Schmidtko, S. Drivers and mechanisms of ocean deoxygenation. *Nat. Geosci.* **11**, 467–473 (2018).
- Oschlies, A. et al. Patterns of deoxygenation: sensitivity to natural and anthropogenic drivers. *Philos. Trans. R. Soc. A: Math. Phys. Eng. Sci.* **375**, 20160325 (2017).
- Hobday, A. J. et al. A hierarchical approach to defining marine heatwaves. *Prog. Oceanogr.* **141**, 227–238 (2016).
- Frölicher, T. L., Fischer, E. M. & Gruber, N. Marine heatwaves under global warming. *Nature* **560**, 360–364 (2018).
- Oliver, E. C. J. et al. Longer and more frequent marine heatwaves over the past century. *Nat. Commun.* **9**, 1–12 (2018).
- Amaya, D. J., Miller, A. J., Xie, S. P. & Kosaka, Y. Physical drivers of the summer 2019 North Pacific marine heatwave. *Nat. Commun.* **11**, 1–10 (2020).
- Oliver, E. C. J. et al. Marine heatwaves. *Annu. Rev. Mar. Sci.* **13**, 313–342 (2021).
- Heinze, C. et al. Reviews and syntheses: abrupt ocean biogeochemical change under human-made climatic forcing – warming, acidification, and deoxygenation. Preprint at <https://doi.org/10.5194/bg-2023-182> (2023).
- Atkins, J., Andrews, O. & Frenger, I. Quantifying the contribution of ocean mesoscale eddies to low oxygen extreme events. *Geophys. Res. Lett.* e2022GL098672 <https://doi.org/10.1029/2022GL098672> (2022).
- Mogen, S. C. et al. Ocean biogeochemical signatures of the North Pacific Blob. *Geophys. Res. Lett.* **49**, e2021GL096938 (2022).

23. Brauko, K. M. et al. Marine heatwaves, sewage and eutrophication combine to trigger deoxygenation and biodiversity loss: a SW Atlantic case study. *Front. Mar. Sci.* **7**, 590258 (2020).
24. Safonova, K., Meier, H. E. M. & Gröger, M. Summer heatwaves on the Baltic Sea seabed contribute to oxygen deficiency in shallow areas. *Commun. Earth Environ.* **5**, 106 (2024).
25. Boyd, P. W. & Brown, C. J. Modes of interactions between environmental drivers and marine biota. *Front. Mar. Sci.* **2**, 9 (2015).
26. Laufkötter, C., John, J. G., Stock, C. A. & Dunne, J. P. Temperature and oxygen dependence of the remineralization of organic matter. *Glob. Biogeochem. Cycles* **31**, 1038–1050 (2017).
27. Mattiasen, E. G. et al. Effects of hypoxia on the behavior and physiology of kelp forest fishes. *Glob. Change Biol.* **26**, 3498–3511 (2020).
28. Tomasetti, S. J. et al. Warming and hypoxia reduce the performance and survival of northern bay scallops (*Argopecten irradians* irradians) amid a fishery collapse. *Glob. Change Biol.* 1–16 <https://doi.org/10.1111/gcb.16575> (2023).
29. Tran, L. L. & Johansen, J. L. Seasonal variability in resilience of a coral reef fish to marine heatwaves and hypoxia. *Glob. Change Biol.* **29**, 2522–2535 (2023).
30. Danabasoglu, G. et al. The community earth system model Version 2 (CESM2). *J. Adv. Model. Earth Syst.* **12**, e2019MS001916 (2020).
31. Zscheischler, J. & Seneviratne, S. I. Dependence of drivers affects risks associated with compound events. *Sci. Adv.* **3**, 1–11 (2017).
32. Ridder, N. N. et al. Global hotspots for the occurrence of compound events. *Nat. Commun.* **11**, 1–10 (2020).
33. Woolway, R. I., Kraemer, B. M., Zscheischler, J. & Albergel, C. Compound hot temperature and high chlorophyll extreme events in global lakes. *Environ. Res. Lett.* **16**, 124066 (2021).
34. Hatton, I. A., Heneghan, R. F., Bar-On, Y. M. & Galbraith, E. D. The global ocean size spectrum from bacteria to whales. *Sci. Adv.* **7**, 1–13 (2021).
35. Le Grix, N., Cheung, W. L., Reygondeau, G., Zscheischler, J. & Frölicher, T. L. Extreme and compound ocean events are key drivers of projected low pelagic fish biomass. *Glob. Change Biol.* **29**, 6478–6492 (2023).
36. Pilo, G. S., Holbrook, N. J., Kiss, A. E. & Hogg, A. M. C. Sensitivity of marine heatwave metrics to ocean model resolution. *Geophys. Res. Lett.* **46**, 14604–14612 (2019).
37. Guo, X. et al. Threat by marine heatwaves to adaptive large marine ecosystems in an eddy-resolving model. *Nat. Clim. Change* **12**, 179–186 (2022).
38. Wu, Z. & Huang, N. E. Ensemble empirical mode decomposition: a noise-assisted data analysis method. *Adv. Adapt. Data Anal.* **01**, 1–41 (2009).
39. Ji, F., Wu, Z., Huang, J. & Chassignet, E. P. Evolution of land surface air temperature trend. *Nat. Clim. Change* **4**, 462–466 (2014).
40. Huang, J., Xie, Y., Guan, X., Li, D. & Ji, F. The dynamics of the warming hiatus over the Northern Hemisphere. *Clim. Dyn.* **48**, 429–446 (2017).
41. Li, C. et al. The variability of air-sea O₂ flux in CMIP6: implications for estimating terrestrial and oceanic carbon sinks. *Adv. Atmos. Sci.* **39**, 1271–1284 (2022).
42. Holbrook, N. J. et al. A global assessment of marine heatwaves and their drivers. *Nat. Commun.* **10**, 1–14 (2019).
43. Holbrook, N. J. et al. Keeping pace with marine heatwaves. *Nat. Rev. Earth Environ.* **1**, 482–493 (2020).
44. Bopp, L., Le Quéré, C., Heimann, M., Manning, A. C. & Monfray, P. Climate-induced oceanic oxygen fluxes: implications for the contemporary carbon budget. *Glob. Biogeochem. Cycles* **16**, 6–16–13 (2002).
45. Huang, J. et al. The global oxygen budget and its future projection. *Sci. Bull.* **63**, 1180–1186 (2018).
46. Chen, X. & Tung, K. K. Global surface warming enhanced by weak Atlantic overturning circulation. *Nature* **559**, 387–391 (2018).
47. Boyer, T. P. et al. *World Ocean Database 2018*. (NOAA Atlas NES-DIS, 2018).
48. Banzon, V., Smith, T. M., Mike Chin, T., Liu, C. & Hankins, W. A long-term record of blended satellite and in situ sea-surface temperature for climate monitoring, modeling and environmental studies. *Earth Syst. Sci. Data* **8**, 165–176 (2016).
49. Sharp, J. D. et al. GOBAI-O 2: temporally and spatially resolved fields of ocean interior dissolved oxygen over nearly 2 decades. *Earth Syst. Sci. Data* **15**, 4481–4518 (2023).
50. Eyring, V. et al. Overview of the Coupled Model Intercomparison Project Phase 6 (CMIP6) experimental design and organization. *Geosci. Model Dev.* **9**, 1937–1958 (2016).
51. Burger, F. A., Terhaar, J. & Frölicher, T. L. Compound marine heatwaves and ocean acidity extremes. *Nat. Commun.* **13**, 4722 (2022).
52. Liu, X. et al. The role of seasonality in the spread of COVID-19 pandemic. *Environ. Res.* **195**, 110874 (2021).
53. Amaya, D. et al. Marine heatwaves need clear definitions so coastal communities can adapt. *Nature* **616**, 29–32 (2023).

Acknowledgements

The authors thank the NOAA National Centers for Environmental Information (NCEI) for collecting and providing the temperature and oxygen profiles in World Ocean Database. The simulations and data analysis are supported by Supercomputing Center of Lanzhou University. This work was jointly supported by the National Science Foundation of China (Grant Nos. 41991231, 42488201, 42375021), the Lanzhou Special Fund for Talent Program, the China 111 project (Grant No. B13045), the Fundamental Research Funds for the Central Universities (Grant No. lzujbky-2024-pd06) and the Postdoctoral Fellowship Program of CPSF (Grant No. GZC20231000).

Author contributions

The study was designed by C.L. and J.H. The simulations and analysis were conducted by C.L., Y.H. and L.D. The figures were produced by C.L., Y.X. and X.L. All authors contributed ideas and discussed the results. C.L. wrote the initial draft, with all authors contributing to the writing.

Competing interests

The authors declare no competing interests.

Additional information

Supplementary information The online version contains supplementary material available at <https://doi.org/10.1038/s41467-024-51323-8>.

Correspondence and requests for materials should be addressed to Jianping Huang.

Peer review information *Nature Communications* thanks Nathaniel Bindoff and Friedrich Burger for their contribution to the peer review of this work. A peer review file is available.

Reprints and permissions information is available at <http://www.nature.com/reprints>

Publisher's note Springer Nature remains neutral with regard to jurisdictional claims in published maps and institutional affiliations.

Open Access This article is licensed under a Creative Commons Attribution-NonCommercial-NoDerivatives 4.0 International License, which permits any non-commercial use, sharing, distribution and reproduction in any medium or format, as long as you give appropriate credit to the original author(s) and the source, provide a link to the Creative Commons licence, and indicate if you modified the licensed material. You do not have permission under this licence to share adapted material derived from this article or parts of it. The images or other third party material in this article are included in the article's Creative Commons licence, unless indicated otherwise in a credit line to the material. If material is not included in the article's Creative Commons licence and your intended use is not permitted by statutory regulation or exceeds the permitted use, you will need to obtain permission directly from the copyright holder. To view a copy of this licence, visit <http://creativecommons.org/licenses/by-nc-nd/4.0/>.

© The Author(s) 2024